Observation of supercurrent in PbIn-graphene-PbIn Josephson junction

Dongchan Jeong,[1] Jae-Hyun Choi,[1] Gil-Ho Lee,[1] Sanghyun Jo,[1,2] Yong-Joo Doh,[3,*] and Hu-Jong Lee[1,2,†]

[1]*Department of Physics, Pohang University of Science and Technology, Pohang 790-784, Republic of Korea*

[2]*National Center for Nanomaterials Technology, Pohang 790-784, Republic of Korea*

[3]*Department of Display and Semiconductor Physics, Korea University Sejong Campus, Jochiwon, Chungnam 339-700, Republic of Korea*

(Received 24 September 2010; revised manuscript received 23 January 2011; published 2 March 2011)

Superconductor-graphene-superconductor (SGS) junction provides a unique platform to study relativistic electrodynamics of Dirac fermions in graphene combined with proximity-induced superconductivity. We report the observation of the Josephson effect in proximity-coupled superconducting junctions of graphene in contact with $Pb_{1-x}In_x$ ($x = 0.07$) electrodes for temperatures as high as $T = 4.8$ K, with a large value of I_cR_N ($\sim$255 μ V). This demonstrates that $Pb_{1-x}In_x$ SGS junction would facilitate the development of the superconducting quantum information devices and superconductor-enhanced phase-coherent transport of graphene.

DOI: 10.1103/PhysRevB.83.094503 PACS number(s): 74.45.+c, 74.50.+r, 74.78.Na, 72.80.Vp

I. INTRODUCTION

Properties of graphene, a monolayer honeycomb lattice of carbon atoms, have been investigated intensively ever since it was first discovered by the mechanical exfoliation.[1,2] To date, experimental and theoretical studies have mainly been focused on features arising from its unique band structure, described by the relativistic Dirac equation.[3–5] The chiral nature of charge carriers in graphene is revealed in transport measurements of the half-integer quantum Hall effect,[6–8] weak localization,[9,10] and Klein tunneling,[11,12] etc.

A superconductor-graphene (SG) hybrid system, such as a superconductor-graphene-superconductor (SGS) junction or an SG interface, provides an ideal platform to investigate the relativistic nature of Dirac fermions combined with superconductivity.[13,14] Instead of the retroreflection of carriers in an ordinary superconductor–normal-metal interface, an SG interface is theoretically predicted to show the specular reflection of chiral quasiparticle carriers.[14] The specular reflection of carriers near the Dirac point can be more easily observed if superconducting material with a large superconducting energy gap is employed for the electrodes because the effect of unexpected charge doping near the Dirac point is minimized. Moreover, phase-coherent transport in graphene of quasiparticles with the energy below the superconducting energy gap can be enhanced significantly due to the condensation of electrons in superconductor into a single macroscopic quantum state. This property can be applied for mesoscopic phase interferometer[15] of graphene. A large superconducting energy gap with a high transition temperature T_c also provides a potential advantage for qubit application of graphene, where a Josephson element is operable at high temperatures. Yet, previous experimental studies have mainly been focused on SGS junctions with Al electrodes,[16–19] which have a relatively small superconducting gap energy of $2\Delta_{Al} \sim 250$ μeV (this value is smaller than the bulk value of $\sim$340 μ eV) and low T_c ($\sim$1 K). For Al-based SGS-junction devices measurements with high sensitivity at low temperatures below 1 K are required to overcome the external noise. Although other experimental results of SGS junctions employing W and Pt/Ta as superconducting electrodes have been reported,[20,21] either the supercurrent was not clearly seen[20] or it was achieved only after heavy annealing of the sample.[21] Thus, realizing SGS Josephson coupling employing a new superconducting material with a higher superconducting energy gap, as in this study, can be regarded as significant progress in studies of superconducting-proximity effect in graphene.

We report on the fabrication and measurements of the SGS Josephson junctions employing $Pb_{0.93}In_{0.07}$ as the superconducting-electrode material with a higher T_c of 7.0 K. The $Pb_{1-x}In_x$-based SGS junction exhibits the supercurrent up to $T \sim 4.8$ K above the liquid-helium temperature, which is the highest operation temperature of an SGS junction reported to date. The junction response to the external magnetic or microwave field manifests the genuine Josephson characters expected by the theory.[22] Extensive studies on the electrical transport properties of our SGS junctions, which depend on the bias (V) and the back-gate voltage (V_{BG}), reveal the superconducting energy gap of $2\Delta_{PbIn} \sim 2.2$ meV. It is an order of magnitude higher than that of Al. The studies also reveal the subgap structures of differential conductance (dI/dV) induced by the multiple Andreev reflection.[23] Thus, SGS junctions consisting of $Pb_{1-x}In_x$ superconducting electrodes lead to the superior device performance over the previous Al-based SGS junctions.

II. SAMPLE PREPARATION

We used $Pb_{1-x}In_x$ alloy instead of pure Pb as the superconducting-electrode material to minimize the granularity of electrodes while their T_c remains almost intact. Both lead (Pb) and indium (In) are type-I superconductors with different superconducting transition temperatures ($T_{c,\mathrm{Pb}} = 7.19$ K, $T_{c,\mathrm{In}} = 3.40$ K). The $Pb_{1-x}In_x$ alloy, however, makes a type-II superconductor, T_c and critical magnetic field of which vary depending on the composition ratio.[24] The $Pb_{1-x}In_x$ film was thermally deposited at the rate of 0.7 nm/s in the base pressure of 6×10^{-7} Torr.

Atomic force microscope (AFM) measurement reveals that the $Pb_{1-x}In_x$ ($x = 0.04, 0.07$, and 0.10) films exhibit a granular structure with the grain diameter of $300 \sim 400$ nm and the root-mean-square roughness of 9.5 nm [see the inset of Fig. 1(a)]. It should be noted that the $Pb_{1-x}In_x$ film on the graphene layer gets significantly thinner than the outer parts, which is probably caused by the fact that the $Pb_{1-x}In_x$ is more mobile on graphene than directly on the oxidized Si substrate.[25] T_c of

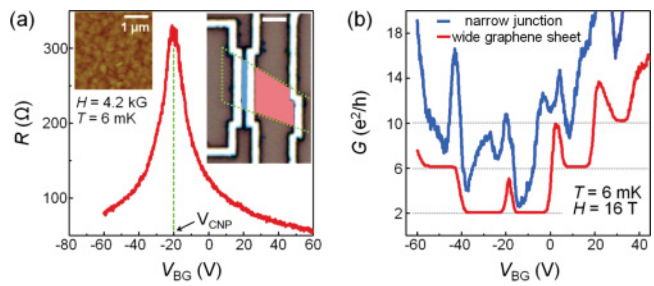

FIG. 1. (Color online) (a) Gate-voltage dependence of the junction resistance obtained from the $Pb_{0.93}In_{0.07}$-based SGS junction in the normal state in a perpendicular field of $H = 4.2$ kOe and at $T = 6$ mK. The charge neutrality point ($V_{CNP} = -20$ V) is indicated by an arrow. Left inset: topographic AFM image of the $Pb_{0.93}In_{0.07}$ film showing granular morphology. Right inset: optical microscope image of the device. The dotted line denotes the boundary of the monolayer graphene. The narrow colored region indicates the 300-nm spacing of graphene layer between two $Pb_{0.93}In_{0.07}$ electrodes. The wide colored region of graphene layer used for the measurement of the quantum Hall plateaus, respectively. (b) Gate-voltage-dependent conductance of the narrow junction and the wide graphene sheet with H =16 T at T = 6 mK. The dotted line corresponds to $G = \nu e^2/h$ ($\nu = 2,6,10,\ldots$).

$Pb_{1-x}In_x$ film on graphene is sensitive to its thickness, which in turn is responsible for the superconducting proximity effect in graphene. The thickness and the atomic composition of $Pb_{1-x}In_x$ electrodes were adjusted so as to obtain the highest value of T_c of 7.0 K for $Pb_{1-x}In_x$ film. The contact resistance obtained from three-probe measurement configuration was in the range of $1 - 15\ \Omega\,\mu\mathrm{m}^2$ in most of our devices and it was insensitive to the temperature change.

Monolayer graphene was mechanically exfoliated from the natural graphite by using Scotch brand tape and transferred on a highly electron-doped silicon substrate covered with a 300-nm-thick oxidized-silicon layer. The carrier density in the graphene was tuned by using the silicon substrate as a back gate. The 900-nm-wide electrode of $Pb_{0.93}In_{0.07}$/Au (200/10 nm in thickness) double layer was formed on top of a graphene flake with a spacing (L) of 300 nm between the electrodes. In this study, two sets of dilution fridges (Leiden Cryogenics Model MNK 126-500 and Oxford Instruments Model AST) were employed. The latter was used to measure the microwave response of the SGS junction. For the low-noise measurements, two-stage RC filters (cut-off frequency ~30 kHz) and π filters were connected in series with the measurement leads and a low-frequency (~13.3 Hz) conventional lock-in technique was adopted for the measurement of dynamic conductance dI/dV.

III. RESULTS AND DISCUSSION

Figure 1(a) shows the back-gate voltage (V_{BG}) dependence of the junction resistance at $T = 6$ mK, obtained by quenching the superconductivity of $Pb_{0.93}In_{0.07}$ electrodes in an external magnetic field of $H = 0.42$ T. It reveals the charge neutrality point (V_{CNP}) at $V_{BG} = -20$ V. The carrier mobility and the mean-free path are estimated to be $\mu \sim 1400\ \mathrm{cm^2/V/sec}$ and $l \sim 24$ nm, respectively, for $\Delta V_{BG} = -30$ V, where $\Delta V_{BG} \equiv V_{BG} - V_{CNP}$. The spacing of the graphene junction between two Al electrodes is an order of magnitude longer than the carrier mean-free path ($L > l$) in the graphene, which implies that all the data should be analyzed in terms of the proximity-junction model in a diffusive limit.

The single-layered-ness of graphene is confirmed by the quantized Hall conductance measured in a high-magnetic field of $H = 16$ T. In a quantum-Hall regime, the conductance plateaus of $G = \nu e^2/h$ with the quantized filling factor of $\nu =$ 2, 6, 10 are expected for the monolayer graphene,[1,2] where h is Planck's constant. In a two-probe configuration adopted in this study with the invasive electrode contacts over the graphene layer, however, the Hall conductivity (σ_{xy}) is mixed with the longitudinal conductivity (σ_{xx}), which is dependent on the aspect ratio ($\zeta = L/W$) of the graphene layer in the junction area.[26,27] Thus, conductance dips take place for the SGS junction with $\zeta = 0.05$, while the neighboring junction with $\zeta \sim 0.9$ on the same graphene layer exhibits the quantized conductance plateaus, as shown in Fig. 1(b).

The resistive transition of the $Pb_{0.93}In_{0.07}$ electrodes shows an onset of the superconductivity at $T_{c,\mathrm{onset}} = 7.15$ K, while the electrodes become fully superconducting below $T_c = 7.0$ K [see the inset of Fig. 2(a)]. The Josephson coupling is established through the graphene layer in the SGS junction below T_c of $Pb_{0.93}In_{0.07}$ electrodes. In Fig. 2(a), the current-voltage (I-V) curve obtained at the base temperature ($T =$ 6 mK) shows a sharp switching from a dissipationless to a resistive state at a critical current ($I_c \sim 3.0\ \mu$A). A reverse switching occurs at a retrapping current ($I_R \sim 0.8\ \mu$A), which yields the clear hysteretic behavior. The ambient magnetic field

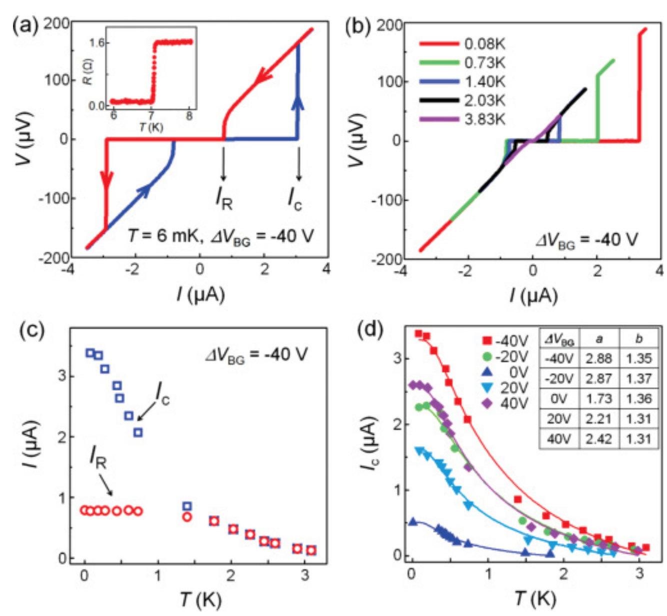

FIG. 2. (Color online) (a) Current-voltage (I-V) characteristic curve measured at $\Delta V_{BG} = -40$ V with increasing and decreasing bias current. The critical (I_c) and the retrapping (I_R) currents are indicated. Inset: resistance vs temperature (R-T) curve of a $Pb_{1-x}In_x$ electrode, revealing T_c=7.0 K. (b) I-V curves with five different temperatures at $\Delta V_{BG} = -40$ V. (c) T dependencies of I_c and I_R for $\Delta V_{BG} = -40$ V. (d) $I_c - T$ curves for different back-gate voltages. The solid lines are the theoretical fits explained in the text.

was canceled by applying a compensation field of $H = 1.84$ Oe, at which I_c was maximized.

Progressive evolution of the I-V characteristics with temperature is displayed in Fig. 2(b), where the bias current is swept from negative to positive polarity. The asymmetry in I-V curves represents the occurrence of hysteresis. With increasing T, I_c becomes smaller and the hysteresis is reduced. It is noted that I_c remains finite for T as high as 3.83 K. After the thermal recycling (i.e., switching the cryostat from Leiden Cryogenics Model MNK 126-500 to Oxford Instruments Model AST), I_c became observable up to 4.8 K above the liquid-helium temperature (see the supplementary information).[25] The corresponding critical current density, $J_c(0) \sim 9.4 \times 10^{-3}$ A/cm, is a record high obtained from SGS junctions to date.

Typical temperature dependencies of I_c and I_R are displayed in Fig. 2(c) for $V_{\mathrm{BG}} = -40$ V. I_c decreases rapidly with increasing temperature but I_R remains almost constant up to $T = 1.77$ K, at which the hysteresis disappears (or I_c becomes equal to I_R). Similar T dependence of I_c is obtained for different gate voltages, as illustrated in Fig. 2(d). The overall $I_c - T$ curves well fit the diffusive Josephson-junction behavior in a long junction regime,[28]

$$eI_cR_N = aE_{\mathrm{Th}}\left[1 - b\exp\left(\frac{-aE_{\mathrm{Th}}}{3.2k_BT}\right)\right], \tag{1}$$

where E_{Th} is the Thouless energy and a and b are fitting parameters. From the $R - V_{\mathrm{BG}}$ curve in Fig. 1(a), $E_{\mathrm{Th}}(=\hbar D/L^2$; $\hbar \equiv h/2\pi)$ is estimated to be about 90 μeV for V_{BG} sufficiently away from the CNP ($\Delta V_{\mathrm{BG}} = -40$ V) and is weakly dependent on ΔV_{BG}. Here, D $(= v_F l/2$; v_F is the Fermi velocity) is the diffusion constant of graphene. In comparison with the theoretical expectation of $a = 10.8$ and $b = 1.30$, in a long junction limit of $E_{\mathrm{Th}}/\Delta_{\mathrm{PbIn}} \to 0$, the best-fit values of parameters a and b of our device turn out to be 1.7 - 2.9 and $\sim$1.3, respectively, with $E_{\mathrm{Th}}/\Delta_{\mathrm{PbIn}} = 0.083$. Our PbIn-based SGS junction, however, corresponds to an intermediate regime between the long- and short-junction limits (see the discussion below), where a smaller value of a is expected from the theoretical calculation of Ref. 28. This may lead to the reduction of the parameter a in our junction. We note that the onset temperature (T^*) of a finite I_c is strongly dependent on the gate voltage, resulting in the highly increased T^* and much larger $I_c(T = 0)$ as well for the gate voltages further away from V_{CNP}. This is attributed to a competition between the Josephson coupling energy ($E_J = \hbar I_c/2e$) and thermal fluctuations. Due to a small value of I_c near V_{CNP}, the supercurrent is vulnerable to the thermal fluctuation, which results in the reduction of T^*.

Gate-voltage dependencies of I_c and I_R at $T = 6$ mK are displayed in Fig. 3(a), the magnitude of which increases monotonously with ΔV_{BG}. As observed previously in SGS junctions[16] the V_{BG} dependence of I_c correlates with the V_{BG} dependence of the normal-state conductance $G(V_{\mathrm{BG}})$ represented by the black curve. The significant difference between the two ($I_c > I_R$) indicates that the hysteretic I-V curves prevail over the whole V_{BG} even including V_{CNP}. Similar hysteresis is observed in various proximity-coupled Josephson junctions consisting of normal metals,[29] semiconductor nanowires,[30,31] and carbon nanotubes.[32] In a resistively and capacitively shunted junction (RCSJ) model,[22] which is a

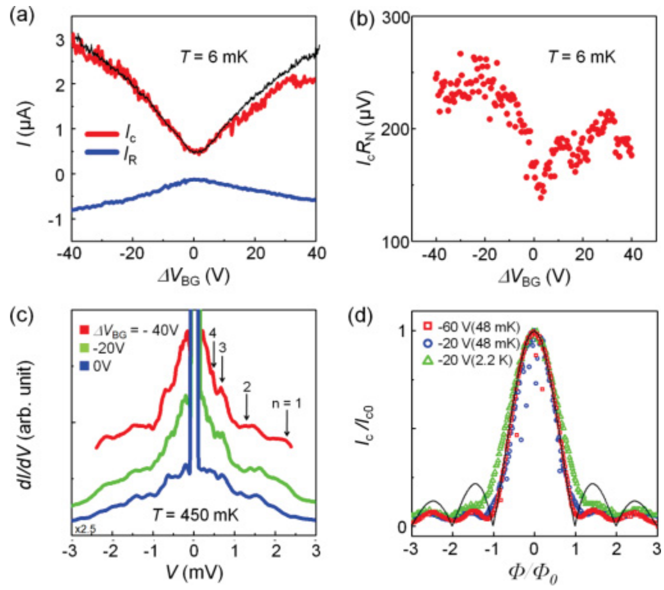

FIG. 3. (Color online) (a) Gate-voltage dependence of I_c (upper curve) and I_R (lower curve) at $T = 6$ mK with bias current swept from negative to positive polarity. (b) I_cR_N product as a function of the back-gate voltage. (c) dI/dV vs V curves with varying $\Delta V_{\mathrm{BG}} = 0$, -20, -40 V from bottom to top. The conductance with $\Delta V_{\mathrm{BG}} = 0$ V is magnified by 2.5 times for the sake of clarity. The arrows indicate the subgap structures corresponding to the voltage of $V_n = 2\Delta_{\mathrm{PbIn}}/ne$ ($n = 1, 2, 3, 4$). (d) The normalized critical current (I_c) as a function of magnetic flux (Φ) measured at $\Delta V_{\mathrm{BG}} = -60$ V and -20 V for $T =$ 48 mK and -20 V for $T = 2.2$ K. The maximum critical currents (I_{c0}) are $I_{c0} = 5.8$, 2.8, 0.8 μA for ΔV_{BG} (T)= -60 (0.048 K), -20 (0.048 K), and -20 (2.2 K) V, respectively. The black curve represents a calculation result of an ideal Fraunhofer pattern (see text).

qualitative model for the Josephson junction, the hysteresis can be explained by the presence of a finite junction capacitance. Although the geometric capacitance (C) is supposed to be negligible in the SGS junction, the effective capacitance (C_{eff} $= \hbar/R_NE_{\mathrm{Th}}$) can be suggested by replacing the quasiparticle characteristic time ($\tau = R_NC$) by the quasiparticle diffusion time in graphene between the electrodes ($\tau_D = \hbar/E_{\mathrm{Th}}$),[33] where R_N is the junction resistance in the normal state. Because of the gate-voltage independence of E_{Th}, $C_{\mathrm{eff}} = 88$ fF at $\Delta V_{\mathrm{BG}} = -40$ V is inversely proportional to R_N. The quality factor of the junction, which is defined as $Q =$ $(2eI_cR_N/E_{\mathrm{Th}})^{1/2}$ in terms of C_{eff}, varies in the range of $Q =$ 1.8–2.3, depending on ΔV_{BG}. The approximate expression of $Q \sim I_c/I_R$ yields a comparable result of 3.4–4.5, as can be estimated from Fig. 3(a). This supports our interpretation of the appearance of the hysteresis in terms of the effective capacitance C_{eff}.

The I_cR_N product, which is a figure of merit for a Josephson junction, is given in Fig. 3(b) as a function of ΔV_{BG}. The maximum I_cR_N value reaches 255 μV for $\Delta V_{\mathrm{BG}} = -40$ V and it reduces to 145 μV at V_{CNP}. The ratio of the maximum I_cR_N product to the superconducting gap energy turns out to be $eI_cR_N/\Delta_{\mathrm{PbIn}} = 0.23$, where the value of $\Delta_{\mathrm{PbIn}} = 1.1$ meV determined by the multiple Andreev reflection (to be discussed below) is adopted. Combining with the ratio of $E_{\mathrm{Th}}/\Delta_{\mathrm{PbIn}} =$ 0.083 obtained from the $I_c - T$ curves in Fig. 2, the value of

$eI_cR_N/\Delta_{\mathrm{PbIn}}$ indicates that our PbIn-based SGS junction is in the intermediate regime between the short ($E_{\mathrm{Th}}/\Delta_{\mathrm{PbIn}} > 1$) and the long ($E_{\mathrm{Th}}/\Delta_{\mathrm{PbIn}} < 0.01$) junction limits. According to Ref. 28, the ratio of $E_{\mathrm{Th}}/\Delta_{\mathrm{PbIn}} = 0.083$ of our device should correspond to $eI_cR_N/\Delta_{\mathrm{PbIn}} \sim 0.5$ in the zero-temperature limit. The reduction of I_cR_N of our device below the expected value may be attributed to the suppression of I_c due to the thermal fluctuations and/or incomplete filtering of the external noise. It should be noted that the observed variation of I_cR_N with ΔV_{BG} can be attributed to V_{BG} dependence of E_{Th}, except for the region of V_{BG} close to the CNP ($|\Delta V_{\mathrm{BG}}| < 10$ V) where the carrier density strongly fluctuates due to the presence of electron-hole puddles.

When the highly transparent contact forms at the normal-metal–superconductor (NS) interface, the Andreev reflection process[23,34] takes place, where an incident electron from the normal metal with energy below $2\Delta_{\mathrm{PbIn}}$ is reflected as a hole and a Cooper pair propagates into the superconductor, or vice versa. In an SNS junction a quasiparticle in N, accelerated by potential difference eV_n, can be Andreev-reflected multiple times until its energy exceeds $2\Delta_{\mathrm{PbIn}}$. This multiple Andreev reflection (MAR) is responsible for the subgap conductance peaks occurring at voltages of $V_n = 2\Delta_{\mathrm{PbIn}}/ne$, where n is an integer, as shown in Fig. 3(c). The corresponding superconducting energy gap of $\mathrm{Pb_{0.93}In_{0.07}}$ electrodes is estimated to be $2\Delta_{\mathrm{PbIn}} = 2.2$ meV, which is comparable to the bulk value of 2.7 meV. The subgap structures are evident at the constant V_n values for different gate voltages and become clearer for V_{BG} away from V_{CNP}. This is attributed to a longer phase coherence length of quasiparticles in a higher-doped region.[35]

Direct evidence of the genuine Josephson coupling through the graphene layer, rather than any artifact such as an inadvertent formation of microbridge of diffused $\mathrm{Pb_{1-x}In_x}$ electrodes, is provided by a periodic modulation of I_c in a perpendicular magnetic field, i.e., so-called Fraunhofer pattern.[22] For a conventional Josephson junction, $I_c(H)$ exhibits local minima for integer magnetic flux quanta through the junction area except for $H = 0$. Figure 3(d) shows the magnetic-field dependence of I_c for different V_{BG} and T. At very low temperature of $T = 48$ mK, the periodic oscillations of $I_c(H)$ is clearly manifested with the H period of $H_0 = \Phi_0/A = \Phi_0/[(L+2\lambda)W] \sim 2.8$ Oe, where $\Phi_0 = h/2e$ is the magnetic-flux quantum, W is the junction width, and λ is the London penetration depth of the superconducting $\mathrm{Pb_{0.93}In_{0.07}}$ electrodes.[19] The theoretical prediction follows the relation[22] of $I_c(H) = I_c(0)\sin[2\pi(\Phi/\Phi_0)]/(\Phi/\Phi_0)$, which is in good agreement with the experimental results at low-magnetic flux of $\Phi = HA$. The $I_c(H)$ modulation is observable even at the elevated temperature of $T = 2.2$ K. The tunable Josephson coupling with the external magnetic field is very important for superconducting device applications such as SQUID[36] or mesoscopic phase interferometers[15] of graphene.

Another crucial experimental evidence of the genuine Josephson effect is provided by the microwave response of the junction. A Josephson junction, irradiated by a microwave of frequency f, exhibits quantized voltage plateaus (or Shapiro steps) in the I-V curve at discrete bias voltages of $V_n = nhf/2e$,[22] where h is Planck's constant. Figure 4(a) shows I-V curves obtained from the $\mathrm{Pb_{0.93}In_{0.07}}$-based SGS junction under the microwave irradiation of $f = 6$ GHz with varying

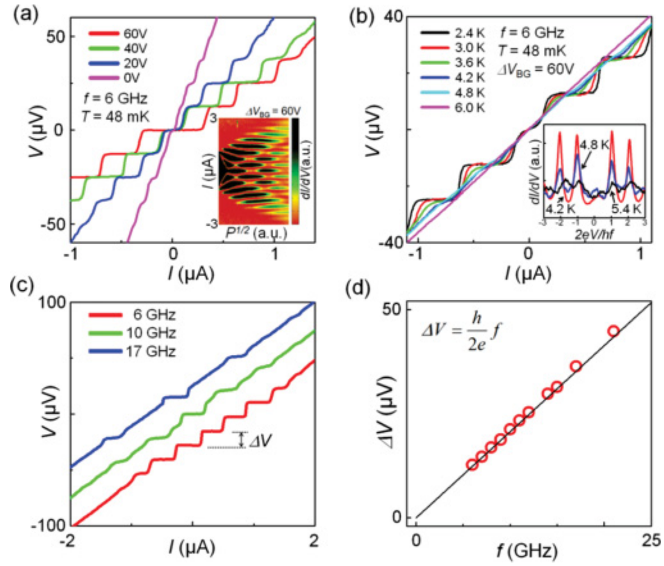

FIG. 4. (Color online) (a) Gate-voltage dependent I-V curves under the irradiation of a microwave of $f = 6$ GHz at $T = 48$ mK. Inset: color-coded plot of dI/dV as a function of I and square root of the microwave power ($P^{1/2}$) at $\Delta V_{\mathrm{BG}} = 60$ V. (b) I-V curves measured at various temperatures under the irradiation of a microwave with $f = 6$ GHz at $\Delta V_{\mathrm{BG}} = 60$ V. Inset: dI/dV-V curve obtained at $T = 4.2$, 4.8, and 5.4 K. The voltage was normalized by $hf/2e$ to clarify the existence of the Shapiro steps at $T = 4.2$ and 4.8 K. (c) $I - V$ characteristic curves at 48 mK and $\Delta V_{\mathrm{BG}} = -60$ V with varying external microwave of frequency $f = 6$ GHz, 10 GHz, and 17 GHz from bottom to top. ΔV is the voltage interval between two different neighboring Shapiro steps. The curves are shifted for clarity. (d) The voltage interval ΔV as a function of microwave frequency f. The solid line shows a good agreement with the ac Josephson relation $\Delta V = hf/2e$.

ΔV_{BG}. The voltage interval between neighboring Shapiro steps is obtained to be $V_n = 12.4$ μV, which is irrespective of ΔV_{BG} and precisely corresponds to the theoretical expectation of $V_n = hf/2e$. The proportionality relation between ΔV_n and f with the slope of $h/2e = 2.07$ μV/GHz is also confirmed in the frequency range of $f = 6$–21 GHz as shown in Figs. 4(c) and 4(d) . The widths of the Shapiro steps in the current axis is quasiperiodically modulated with the microwave power ($P^{1/2}$), as shown in the inset of Fig. 4(a), which resembles the Bessel-function-like behavior.[30] It is surprising to observe the quantized voltage plateaus at the elevated temperature up to $T = 4.8$ K in Fig. 4(b), although the step edges are rounded by thermal fluctuations. The dI/dV-V curves in the inset indicate that the Shapiro steps are almost vanishing only at $T = 5.4$ K.

IV. SUMMARY

In summary, we demonstrate the realization of $\mathrm{Pb_{1-x}In_x}$-based SGS Josephson junctions. Temperature dependence of the critical current and the value of I_cR_N product of our system are well understood by the diffusive Josephson junction model. The dc and ac Josephson effects through the graphene layer are sustained over the liquid helium temperature. Furthermore, the experimental play ground for the graphene-based Josephson junction will be extended to much wider ranges of temperature, bias voltage, and magnetic field to explore the relativistic and superconducting phenomena with a reduction of unintended doping effect near the charge-neutrality point. The previous requirement of ultralow temperatures ($T \ll 1$ K) to observe the supercurrent in the conventional Al-based SGS junctions can be resolved by employing the $Pb_{1-x}In_x$-based junctions, which can be readily generalized for other nanostructures, including carbon nanotubes and semiconductor nanowires. Ultimately, the superior Josephson-junction properties of $Pb_{1-x}In_x$-based junctions would leads to a very crucial step toward the application to graphene-based quantum information devices and gate-tunable Josephson devices.[37–39]

ACKNOWLEDGMENTS

This work was supported by National Research Foundation of Korea (NRF) (for HJL) through Acceleration Research Grant Nos. R17-2008-007-01001-0 and 2009-0083380, and (for YJD) through Grant No. 2010-0008450 (Basic Science Research Program) funded by the Ministry of Education, Science and Technology.

*Corresponding author: yjdoh@korea.ac.kr
†hjlee@postech.ac.kr

[1] K. S. Novoselov, A. K. Geim, S. V. Morozov, D. Jiang, M. I. Katsnelson, I. V. Grigorieva, S. V. Dubonos, and A. A. Firsov, Nature (London) **438**, 197 (2005).
[2] Y. Zhang, Y.-W. Tan, H. L. Stormer, and P. Kim, Nature (London) **438**, 201 (2005).
[3] A. K. Geim and K. S. Novoselov, Nat. Mater. **6**, 183 (2007).
[4] A. K. Geim, Science **324**, 1530 (2009).
[5] A. H. Castro Neto, F. Guinea, N. M. R. Peres, K. S. Novoselov, and A. K. Geim, Rev. Mod. Phys. **81**, 109 (2009).
[6] K. S. Novoselov, Z. Jiang, Y. Zhang, S. V. Morozov, H. L. Stormer, U. Zeitler, J. C. Maan, G. S. Boebinger, P. Kim, and A. K. Geim, Science **315**, 1379 (2007).
[7] J. R. Williams, L. DiCarlo, and C. M. Marcus, Science **317**, 638 (2007).
[8] D.-K. Ki and H.-J. Lee, Phys. Rev. B **79**, 195327 (2009).
[9] F. V. Tikhonenko, D. W. Horsell, R. V. Gorbachev, and A. K. Savchenko, Phys. Rev. Lett. **100**, 056802 (2008).
[10] F. V. Tikhonenko, A. A. Kozikov, A. K. Savchenko, and R. V. Gorbachev, Phys. Rev. Lett. **103**, 226801 (2009).
[11] N. Stander, B. Huard, and D. Goldhaber-Gordon, Phys. Rev. Lett. **102**, 026807 (2009).
[12] A. F. Young and P. Kim, Nat. Phys. **5**, 222 (2009).
[13] C. W. J. Beenakker, Rev. Mod. Phys. **80**, 1337 (2008).
[14] C. W. J. Beenakker, Phys. Rev. Lett. **97**, 067007 (2006).
[15] V. T. Petrashov, V. N. Antonov, P. Delsing, and T. Claeson, Phys. Rev. Lett. **74**, 5268 (1995).
[16] H. B. Heersche, P. Jarillo-Herrero, J. B. Oostinga, L. M. K. Vandersypen, and A. F. Morpurgo, Nature (London) **446**, 56 (2007).
[17] X. Du, I. Skachko, and E. Y. Andrei, Phys. Rev. B **77**, 184507 (2008).
[18] F. Miao, W. Bao, H. Zhang, and C. N. Lau, Solid State Commun. **149**, 1046 (2009).
[19] J.-H. Choi, H.-J. Lee, and Y.-J. Doh, J. Korean Phys. Soc. **57**, 149 (2010).
[20] A. Shailos, W. Nativel, A. Kasumov, C. Collet, M. Ferrier, S. Guéron, R. Deblock, and H. Bouchiat, Europhys. Lett. **79**, 57008 (2007).
[21] C. Ojeda-Aristizabal, M. Ferrier, S. Guéron, and H. Bouchiat, Phys. Rev. B **79**, 165436 (2009).
[22] M. Tinkham, *Introduction to Superconductivity* (McGraw-Hill, New York, 1996).
[23] A. F. Andreev, Zh. Eksp. Teor. Fiz. **46**, 1823 (1964) [Sov. Phys. JETP **19**, 1228 (1964)].
[24] J. E. Evetts and J. M. A. Wade, J. Phys. Chem. Solids **31**, 973 (1970).
[25] See supplemental material at [http://link.aps.org/supplemental/10.1103/PhysRevB.83.094503] for two supplementary figures and detailed explanations.
[26] D. A. Abanin and L. S. Levitov, Phys. Rev. B **78**, 035416 (2008).
[27] J. R. Williams, D. A. Abanin, L. DiCarlo, L. S. Levitov, and C. M. Marcus, Phys. Rev. B **80**, 045408 (2009).
[28] P. Dubos, H. Courtois, B. Pannetier, F. K. Wilhelm, A. D. Zaikin, and G. Schön, Phys. Rev. B **63**, 064502 (2001).
[29] H. Courtois, M. Meschke, J. T. Peltonen, and J. P. Pekola, Phys. Rev. Lett. **101**, 067002 (2008).
[30] Y.-J. Doh, J. A. van Dam, A. L. Roest, E. P. A. M. Bakkers, L. P. Kouwenhoven, and S. De Franceschi, Science **309**, 272 (2005).
[31] J. Xiang, A. Vidan, M. Tinkham, R. M. Westervelt, and C. M. Lieber, Nature Nanotechnology **1**, 208 (2006).
[32] P. Jarillo-Herrero, J. A. van Dam, and L. P. Kouwenhoven, Nature (London) **439**, 953 (2006).
[33] L. Angers, F. Chiodi, G. Montambaux, M. Ferrier, S. Guéron, H. Bouchiat, and J. C. Cuevas, Phys. Rev. B **77**, 165408 (2008).
[34] G. E. Blonder, M. Tinkham, and T. M. Klapwijk, Phys. Rev. B **25**, 4515 (1982).
[35] D.-K. Ki, D. Jeong, J.-H. Choi, H.-J. Lee, and K.-S. Park, Phys. Rev. B **78**, 125409 (2008).
[36] C. Girit, V. Bouchiat, O. Naaman, Y. Zhang, M. F. Crommie, A. Zettl, and I. Siddiqi, Nano Lett. **9**, 198 (2009).
[37] J.-P. Cleuziou, W. Wernsdorfer, V. Bouchiat, T. Ondarçuhu, and M. Monthioux, Nature Nanotechnology **1**, 53 (2006).
[38] A. Eichler, R. Deblock, M. Weiss, C. Karrasch, V. Meden, C. Schönenberger, and H. Bouchiat, Phys. Rev. B **79**, 161407(R) (2009).
[39] G. Liu, Y. Zhang, and C. N. Lau, Phys. Rev. Lett. **102**, 016803 (2009).